European Congress on Computational Methods in Applied Sciences and Engineering
ECCOMAS 2000
Barcelona, 11-14 September 2000

VISCOUS-INVISCID INTERACTION METHOD FOR WING CALCULATIONS

Edith G.M. Coenen*, Arthur E.P. Veldman* and George Patrianakos†

*Department of Mathematics
University of Groningen
P.O. Box 800, 9700 AV Groningen, The Netherlands
Email: edith@math.rug.nl, a.e.p.veldman@math.rug.nl
Web page: http://www.math.rug.nl/∼veldman/cfd-gallery.html

†Department of Aerospace Engineering
University of Bristol
Queens Building, University Walk, BS8 1TR Bristol, United Kingdom
Email: g.patrianakos@bristol.ac.uk

Key words: Viscous-inviscid interaction, boundary layer, three-dimensional flow, quasi-simultaneous coupling scheme, panel method.

Abstract. *A quasi-simultaneous viscous-inviscid coupling method is developed for the calculation of three-dimensional steady incompressible flow over transport wing configurations. The external inviscid flow is computed with a constant-potential (Dirichlet) panel method, constructed from a constant source and doublet distribution over the wing surface and wake. From the used external flow formulation three approximations for the velocity components are derived, required for the fully three-dimensional quasi-simultaneous viscous-inviscid interaction scheme. The viscous layer is described with three integral boundary layer equations, in a Cartesian coordinate system, which are solved simultaneously with the approximations for the external flow by Newton's method. Results are presented for two three-dimensional wing flow cases, including separation, and comparisons are made with two-dimensional viscous-inviscid interaction results.*

1 INTRODUCTION

For wing design and analysis, a computational method that can predict aerodynamic characteristics in an economical and efficient way, is an essential tool in todays time-run society. In the past years a lot of attention has been focused on Navier-Stokes simulation for the generation of solutions over wing configurations. A much simpler and computationally economical alternative, however, is to use viscous-inviscid interaction (VII). VII methods produce results that for most cases of engineering interest compare well with experiment and this at much lower computational cost than Navier-Stokes simulations. Furthermore, VII methods give clear insight into the behaviour of the boundary layer since the integral thicknesses are immediately available.

Despite the success in two dimensions, results obtained with three-dimensional VII are still limited [1]. The development of a three-dimensional VII method proves difficult due to the complexity of the boundary layer equations. In two dimensions the boundary layer equations in integral form are simply given by a set of ordinary differential equations. The three-dimensional integral boundary layer is described by three non-linear partial differential equations, which are fully hyperbolic with three real and distinct characteristics [2].

Recently more interest has been shown in three-dimensional VII. Direct and inverse methods have been investigated for the calculation of three-dimensional flow, see for example [2], [3], [4], [5] and [6]. It was found that in the presence of flow separation these methods run into difficulties. The direct scheme becomes instable and ceases to converge as a singularity is encountered in the boundary layer formulation. The inverse methods overcome these problems, but when significant separation is present the inviscid and viscous solutions are mismatched and an efficient update procedure for rectifying this has yet to be developed. To avoid the use of an update procedure, for flow calculations with regions with strong interaction, a more simultaneous approach is preferred [7].

The quasi-simultaneous coupling scheme, developed by Veldman [8] for two-dimensional subsonic flow, treats the boundary layer and the outer flow simultaneously. The boundary layer equations are solved together with suitable approximations for the external inviscid flow. Furthermore, from two-dimensional work it is known that the quasi-simultaneous method converges much faster and is more robust than existing inverse schemes [1]. Similar advantages are also expected in three-dimensional calculations.

The quasi-simultaneous method has a straightforward extension to three dimensions and is employed here. In three dimensions, quasi-simultaneous coupling was shown to work successfully by Edwards [9] for the calculation of laminar flow over a flat plate with protuberance and by Van der Wees *et al.* [10] for the computation of transonic flow over wing/body configurations on the basis of full potential theory. In the latter case the approximations used for the outer flow were based on thin-aerofoil theory. In this paper more suitable approximations will be derived.

The integral boundary layer equations are determined in a Cartesian coordinate system

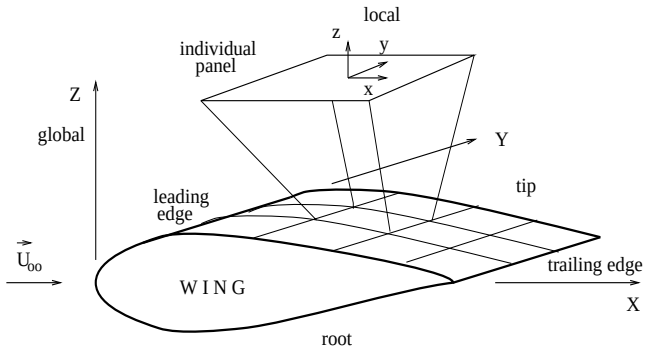

Figure 1: Global (X,Y,Z) and local (x,y,z) Cartesian coordinate systems.

and discretised via an upwind scheme. With this approach, the calculation of cumbersome metric gradients, which have to be evaluated for the traditional boundary layer formulation in a general curvilinear coordinate system, is avoided.

For the computation of the external inviscid flow a constant potential Dirichlet panel method is used, which for irrotational and subsonic flow is much faster than a full potential or Euler method.

The developed program is tested for two wing flow cases, including separation. Results for the quasi-three-dimensional test case are compared with results from a two-dimensional VII program, which follows a similar approach. For the test case with three-dimensional effects present no comparison material is available. It is therefore hoped that the program is soon to be extended to include swept wing calculations on non-orthogonal grids, for which there is more experimental data available for comparison.

2 BOUNDARY LAYER REGION

The boundary layer is described by a set of three turbulent integral boundary layer equations transformed to a local Cartesian coordinate system (x, y, z). The x and y directions lie in the plane tangent to the surface of the boundary layer and z is normal to the plane, as shown in figure 1. The three integral boundary layer equations are:

$$\frac{\partial}{\partial x}(\theta_{xx}q_e^2) + \frac{\partial}{\partial y}(\theta_{xy}q_e^2) + q_e\delta_x^*\frac{\partial u_{e_x}}{\partial x} + q_e\delta_y^*\frac{\partial u_{e_x}}{\partial y} = \tau_{w_x}, \quad (1)$$

$$\frac{\partial}{\partial x}(\theta_{yx}q_e^2) + \frac{\partial}{\partial y}(\theta_{yy}q_e^2) + q_e\delta_x^*\frac{\partial u_{e_y}}{\partial x} + q_e\delta_y^*\frac{\partial u_{e_y}}{\partial y} = \tau_{w_y}, \quad (2)$$

$$\frac{\partial}{\partial x}(u_{e_x}\delta - q_e\delta_x^*) + \frac{\partial}{\partial y}(u_{e_y}\delta - q_e\delta_y^*) = q_e C_E, \quad (3)$$

where δ is the boundary layer thickness, δ_x^* and δ_y^* are the x-, y-displacement thicknesses and θ_{xx}, θ_{xy}, θ_{yx}, and θ_{yy} are the x- and y-momentum thicknesses. The wall shear stress

components are given by τ_{w_x} and τ_{w_y}, and q_e is the total edge velocity, $q_e^2 = u_{e_x}^2 + u_{e_y}^2$, with u_{e_x} and u_{e_y} the local edge velocity components.

Equations (1) and (2) are the x- and y-integral momentum equations and equation (3) is the entrainment equation. The two momentum equations in a Cartesian system are derived in [11]. The entrainment equation can be found, as was shown in two dimensions by Head, by integrating the continuity equation across the boundary layer [12]. The entrainment coefficient C_E describes the (non-dimensional) rate at which fluid from the external inviscid flow enters through the external edge of the boundary layer.

Equations (1), (2) and (3) are hyperbolic and have three real and distinct characteristic directions. These lie between the direction of the streamline and the limiting wall streamline, as is seen in figure 2. One characteristic almost corresponds with the limiting wall streamline as was described in [2].

Closure relations are required to make the problem determinate. The empirical closure relations found are usually based on variables in a streamline coordinate system s, n. To make use of these closure relations, the boundary layer variables in the x, y system need to be transformed to variables in the streamline system. Looking again at figure 2, a relationship between the two systems is easily found in terms of the velocities:

$$\begin{aligned} u_x &= u_s \cos\alpha - u_n \sin\alpha, \\ u_y &= u_s \sin\alpha + u_n \cos\alpha, \end{aligned} \tag{4}$$

where α is the angle between the x and s directions. Furthermore, u_x and u_y are the velocity components in the x, y system and u_s and u_n are the velocity components in the s, n system. With the above relationship the integral thicknesses can be expressed in variables in the s, n system.

For streamwise closure the correlations described in the papers by Ashill *et al.* [13], Green [14] and Houwink and Veldman [15] are to be used, the latter giving a suitable

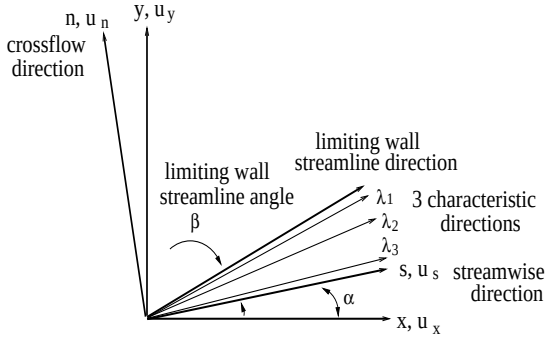

Figure 2: Cartesian and streamline coordinate systems and characteristic directions.

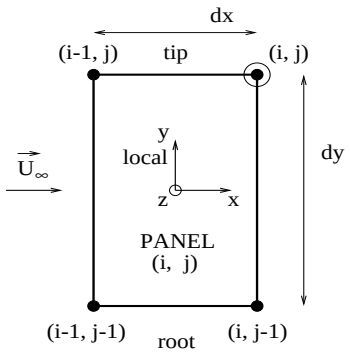

Figure 3: Panel (i, j).

$H - H_1$ relation for separated flow. In this way, the streamwise boundary layer unknowns have been reduced to θ_{ss} and H, where $H = \delta^*_s/\theta_{ss}$, the shape factor. For C_E an empirical expression in three dimensions is not yet available. Therefore, it is assumed that the empirical relationship for C_E in two dimensions also holds for three-dimensional flow [3].

The unknowns in the cross-flow direction are determined by Mager's cross-flow velocity profile, which reduces the total number of boundary layer unknowns to three [3]. These are θ_{ss}, H and β, where β is the limiting streamline angle.

The equations are discretised with an upwind scheme. For the rectangular panel (i, j), defined by the four edge points (x_{i-1j-1}, y_{i-1j-1}), (x_{ij-1}, y_{ij-1}), (x_{ij}, y_{ij}), (x_{i-1j}, y_{i-1j}), as seen in figure 3, the corresponding discretisation of the x-momentum equation (1) in point (x_{ij}, y_{ij}) becomes:

$$\begin{aligned} &\frac{\theta_{xx_{ij}} q^2_{e_{ij}} - \theta_{xx_{i-1j}} q^2_{e_{i-1j}}}{d_{x_{ij}}} + \frac{\theta_{xy_{ij}} q^2_{e_{ij}} - \theta_{xy_{ij-1}} q^2_{e_{ij-1}}}{d_{y_{ij}}} + \\ &\qquad q_{e_{ij}} \delta^*_{x_{ij}} \frac{u_{e_{x_{ij}}} - u_{e_{x_{i-1j}}}}{d_{x_{ij}}} + q_{e_{ij}} \delta^*_{y_{ij}} \frac{u_{e_{x_{ij}}} - u_{e_{x_{ij-1}}}}{d_{y_{ij}}} \quad = \quad \tau_{w_{x_{ij}}}, \end{aligned} \tag{5}$$

where $d_{x_{ij}}$ and $d_{y_{ij}}$ are the lengths of the cell edges in the local x and y direction of panel (i, j).

As the quasi-simultaneous coupling technique is applied, approximations are to be found from the external flow formulation for the velocity components u_{e_X}, u_{e_Y} and u_{e_Z} at the edge of the boundary layer in the global Cartesian coordinate system (X, Y, Z). Via a transformation the local velocity components u_{e_x} and u_{e_y} and the total velocity q_e can be determined.

3 INVISCID FLOW REGION

In the external inviscid region the flow is assumed to be incompressible and irrotational. The inviscid flow field over the wing can then be modelled with three-dimensional potential theory [16]. Along the wing surface a source sheet of strength σ is distributed together with a doublet sheet of strength μ. The latter is also extended into the wake. The total potential Φ is written:

$$\Phi = \Phi_\infty - \frac{1}{4\pi}\iint_{S_B}\frac{\sigma}{r}\mathrm{d}S + \frac{1}{4\pi}\iint_{S_W+S_B}\mu\frac{\partial}{\partial n}\frac{1}{r}\,\mathrm{d}S, \tag{6}$$

where n is the unit normal pointing inside the body surface S_B and outside the wake surface S_W. The freestream potential is given by Φ_∞ and r is the distance between a point at S and a field point (X, Y, Z).

The displacement effect of the boundary layer can be taken into account in equation (6) by modelling an extra viscous source sheet over the surface of the wing and the wake. From the continuity equation and the definition of source strength, σ_{vis} can be found to be:

$$\sigma_{vis} = \frac{\partial}{\partial x}(q_e\delta_x^*) + \frac{\partial}{\partial y}(q_e\delta_y^*). \tag{7}$$

On the wing surface, instead of using a Neumann boundary condition of prescribed normal velocity at the surface, a Dirichlet boundary condition is applied. The total potential inside the body, Φ_i, is specified to be $\Phi_i = \Phi_\infty$ on the boundary. Equation (6) for collocation points inside the body thus becomes:

$$\frac{1}{4\pi}\iint_{S_B+S_W}\mu\frac{\partial}{\partial n}\frac{1}{r}\,\mathrm{d}S = \frac{1}{4\pi}\iint_{S_B}\frac{\sigma_{inv}}{r}\,\mathrm{d}S + \frac{1}{4\pi}\iint_{S_B+S_W}\frac{\sigma_{vis}}{r}\,\mathrm{d}S. \tag{8}$$

The inviscid source strength σ_{inv} can be found from the freestream, and the viscous source strength σ_{vis} is to be given by the boundary layer equations. To determine the problem uniquely, an implicit Kutta condition is used to define the doublet strength in the wake. A set of algebraic equations remains to be solved for the unknown doublet strengths on the surface of the wing.

For the discretisation of the above system the wing body and wake are divided into rectangular surface panel elements as was shown in figure 1. Furthermore, the source and doublet strengths are assumed to be constant over a panel. Relations for the unknown doublet strengths can therefore be determined from equation (8) in the midpoint of each

panel. However, as relations for the velocity components are required for the viscous-inviscid interaction method some further manipulations are performed, using that the doublicity gradients determine the global velocity vector in the end points of the panels [17]. Finally, the above leads to the equations for the global velocity components of the following form:

$$u_{e_{X_{ij}}} = u_{0_{X_{ij}}} + \sum_{k=1}^{N+1} \sum_{l=1}^{M+1} \left[A_{X_{ijkl}} q_{e_{kl}} \delta^*_{x_{kl}} + B_{X_{ijkl}} q_{e_{kl}} \delta^*_{y_{kl}} \right], \tag{9}$$

$$u_{e_{Y_{ij}}} = u_{0_{Y_{ij}}} + \sum_{k=1}^{N+1} \sum_{l=1}^{M+1} \left[A_{Y_{ijkl}} q_{e_{kl}} \delta^*_{x_{kl}} + B_{Y_{ijkl}} q_{e_{kl}} \delta^*_{y_{kl}} \right], \tag{10}$$

$$u_{e_{Z_{ij}}} = u_{0_{Z_{ij}}} + \sum_{k=1}^{N+1} \sum_{l=1}^{M+1} \left[A_{Z_{ijkl}} q_{e_{kl}} \delta^*_{x_{kl}} + B_{Z_{ijkl}} q_{e_{kl}} \delta^*_{y_{kl}} \right], \tag{11}$$

where N is the number of segments into which the contour of the wing section is divided and M is the number of spanwise segments. The velocity components u_{0_X}, u_{0_Y} and u_{0_Z} represent the global undisturbed inviscid velocity and matrices A and B contain the discretisation of the geometry and the differentiation of the viscous source strength (7).

On a flat square grid, $d_{x_{ij}} = d_{y_{ij}}$, the matrix entries of A_X correspond with the matrix entries of B_Y and similar do the matrix entries of A_Y correspond with the matrix entries of B_X. Furthermore, matrices A_X and B_Y can be shown to be diagonally dominant and to have positive values on the main diagonal and negative values on the off-diagonals. These matrix properties will have a positive influence on the iteration process. For the X-velocity in node point (i, j) the most important contributions are then given by the matrix entries $A_{X_{iji-1j}}$, $A_{X_{ijij}}$ and $A_{X_{iji+1j}}$. Similar it is found for the Y-velocity in node point (i, j) that the entries $B_{Y_{ijij-1}}$, $B_{Y_{ijij}}$ and $B_{Y_{ijij+1}}$ contain most of the information.

In the wake similar relations as (9), (10), (11) are determined for the interaction with the boundary layer, using $\vec{U_{e_{ij}}} = \nabla \Phi_{ij}$.

4 QUASI-SIMULTANEOUS COUPLING

The interaction technique applied to couple the set of boundary layer equations (1), (2) and (3) to the inviscid flow equations (9), (10) and (11) is the quasi-simultaneous method [8]. The method is based on the laminar triple-deck theory of Stewartson, who found that near a singularity the thin-shear layer approximations are still valid, but that the inviscid and viscous regions are equally important and should be treated simultaneously.

In the classical direct approach however, derived from asymptotic expansion theory, the external region is calculated first, producing a velocity distribution which is then used for the boundary layer calculations. This method will break down when a singularity occurs. In broad lines the quasi-simultaneous method resembles the direct method. However,

following Stewartson, the quasi-simultaneous method uses simplifications for the inviscid flow, which are solved *simultaneously* with the boundary layer equations. In this way regions with a certain amount of separation can be computed.

A requirement of the quasi-simultaneous method is to find suitable approximations from the external flow equations. These approximations are termed interaction laws and describe the interaction with the boundary layer. The interaction laws are employed in a deficit formula and thus will not influence the final solution. Convergence speed however, depends on how accurately the approximations have been chosen.

Three interaction laws for the global velocity components have been derived from the external flow formulation described. The simple approximations for $u_{e_{X_{ij}}}$, $u_{e_{Y_{ij}}}$ and $u_{e_{Z_{ij}}}$ are taken to be:

$$u_{e_{X_{ij}}} + \tilde{A}_{X_{ijij}} q_{e_{ij}} \delta^*_{x_{ij}} \approx u_{0_{X_{ij}}} + \sum_{\substack{k=i-1 \\ k\neq i}}^{i+1} \left[\tilde{A}_{X_{ijkj}} q_{e_{kj}} \delta^*_{x_{kj}} \right], \tag{12}$$

$$u_{e_{Y_{ij}}} + \tilde{B}_{Y_{ijij}} q_{e_{ij}} \delta^*_{y_{ij}} \approx u_{0_{Y_{ij}}} + \sum_{\substack{l=j-1 \\ l\neq j}}^{j+1} \left[\tilde{B}_{Y_{ijil}} q_{e_{il}} \delta^*_{y_{il}} \right], \tag{13}$$

$$u_{e_{Z_{ij}}} \approx u_{0_{Z_{ij}}}. \tag{14}$$

The approximations for u_{e_X} and u_{e_Y}, contain boundary layer information terms, which for u_{e_Z} are not included. Tridiagonal matrices $\tilde{A}_X$ and $\tilde{B}_Y$ are constructed in the same way as matrices A_X and B_Y, however, only the influence of the four neighbouring panels, which is most important for node point (i, j), is included. The matrix entries $\tilde{A}_{X_{iji-1j}}$, $\tilde{A}_{X_{ijij}}$ and $\tilde{A}_{X_{iji+1j}}$ approximately now correspond to the structure $-1, 2, -1$, which was also found in two-dimensional thin-aerofoil theory [18]. In equations (12) and (13) the summation is done from $k = i - 1$ to $i + 1$, respectively $l = j - 1$ to $j + 1$, with the contribution of $k = i$, respectively $l = j$, written on the left hand side.

For simplification, u_{e_X} only has the contribution from the $q_e\delta^*_x$ part, as the influence of the $q_e\delta^*_y$ part is less important. Velocity u_{e_Y} has its main contribution from $q_e\delta^*_y$. For u_{e_Z} the $q_e\delta^*_x$ and $q_e\delta^*_y$ contributions are very small, the local z-direction being normal to the panels, and have therefore both been omitted. The matrix entries for $\tilde{A}_X$, respectively $\tilde{B}_Y$, have as before in (9) and (10) the correct sign at the main diagonal and a regular behaviour, which will prove favourably towards convergence speed. Only near the trailing edge the structure of the tridiagonal matrices is irregular which is due to the Kutta condition. No coupling will therefore take place in the trailing edge points.

If the operators E, for the external flow calculation, and I, for the interaction law calculation, are introduced, then the interaction law equations in defect formulation,

which are solved together with the boundary layer equations, can be written symbolically as follows:

$$u_{e_X}^{(n+1)} - I_X[\delta_x^{*(n+1)}, \delta_y^{*(n+1)}] = E_X[\delta_x^{*(n)}, \delta_y^{*(n)}] - I_X[\delta_x^{*(n)}, \delta_y^{*(n)}], \quad (15)$$

$$u_{e_Y}^{(n+1)} - I_Y[\delta_x^{*(n+1)}, \delta_y^{*(n+1)}] = E_Y[\delta_x^{*(n)}, \delta_y^{*(n)}] - I_Y[\delta_x^{*(n)}, \delta_y^{*(n)}], \quad (16)$$

$$u_{e_Z}^{(n+1)} - I_Z[\delta_x^{*(n+1)}, \delta_y^{*(n+1)}] = E_Z[\delta_x^{*(n)}, \delta_y^{*(n)}] - I_Z[\delta_x^{*(n)}, \delta_y^{*(n)}]. \quad (17)$$

The right-hand-sight is known and the above three equations together with the three boundary layer equations will produce three new velocities and three new boundary layer values. From the calculated three boundary layer values new displacement thicknesses, δ_x^* and δ_y^*, are determined for a new external inviscid flow calculation. If the scheme converges, it is seen that the I terms drop against each other, therefore not influencing the final solution.

5 SOLUTION METHOD

The constructed discrete equations, consisting of the three boundary layer equations and the three interactions laws, are to be solved simultaneously along a column of panels. Going from root to tip, each panel is treated individually with a pointwise Newton scheme until convergence for the whole column is reached. The solution is then marched downstream along the X-direction, which corresponds approximately with the primary external flow direction.

The unknowns vector $\vec{U}$ to be solved for each pointwise Newton iteration is:

$$\vec{U} = (\theta_{ss}, H, \beta, u_{e_X}, u_{e_Y}, u_{e_Z})^t, \quad (18)$$

which is defined in the node points of the panels. The three boundary layer variables are taken in the streamline coordinate system, whereas the three velocity components are taken in the global Cartesian system.

In the present formulation the angles of the corresponding characteristics have been ignored, implying that all three characteristics are aligned with the freestream for the case of a symmetric unswept wing. It is hoped however, to further improve the method to include the local directions of information flow.

No coupling takes place at the root and tip rows of the wing and boundary conditions need to be supplied. Due to the assumption that the characteristic directions are parallel

to the freestream, a Neumann boundary condition of a zero-spanwise gradient is applied for both rows.

Initial conditions are required for the unknowns vector $\vec{U}$. For this, either a previously calculated nearby solution is used or the solution for two-dimensional turbulent flow over a flat plate is prescribed: $(u_{e_X}, u_{e_Y}, u_{e_Z}) = (1, 0, 0)$, $\theta_{ss} = 0.005/Re^{0.2}$, where Re denotes the Reynolds number, $H = 1.35$ and $\beta = 0$.

The solution at the trailing edge is not calculated with a coupling method, due to the irregular structure of the interaction law matrices. Instead the solution is determined by extrapolation.

The laminar part of the flow is calculated with a two-dimensional Thwaites method, using direct coupling.

6 RESULTS AND DISCUSSION

The above described three-dimensional viscous-inviscid interaction method has been applied to several test cases and some results from two calculations are presented in this section. The first calculation was performed to simulate quasi-two-dimensional unseparated flow. For verification the computed results are compared with a two-dimensional VII program which has been constructed following a similar approach as the present method [19]. The latter calculation was performed to simulate separated flow and demonstrates the three-dimensional capabilities of the method.

For both calculations an unswept NACA0012 wing configuration was used with an aspect ratio of 14. The freestream Reynolds number at which the two cases have been computed, was 9×10^6. Furthermore, a rectangular grid was used with 71 points around the wing section, parallel to the freestream direction, and 9 points in the spanwise direction, as seen in figure 4. Transition was tripped on the upper surface close to the attachment line and on the lower surface at $x/c = 0.35$.

6.1 Quasi-two-dimensional wing flow

The results for the quasi-two-dimensional flow test case have been obtained at an incidence $\alpha = 11^o$. Midwing the flow has the least influence of the tip and root effects, and these results are therefore shown. For comparison results of a two-dimensional VII code have been obtained at an incidence of $\alpha = 10^o$, as at this incidence the pressure distribution corresponds perfectly with the three-dimensional results at 11^o, displayed in figure 5.

In figure 6 a close up is shown of the trailing edge region. It is seen that the Kutta condition of the panel method is not very accurately modelled. The upper and lower trailing edge pressures are different at the trailing edge. Smoothing of the external pressure distribution was therefore needed, to obtain interactive results that do fulfil the Kutta condition of equivalent upper and lower trailing edge pressures.

In figure 7 the streamwise momentum thickness results are compared and it is clear

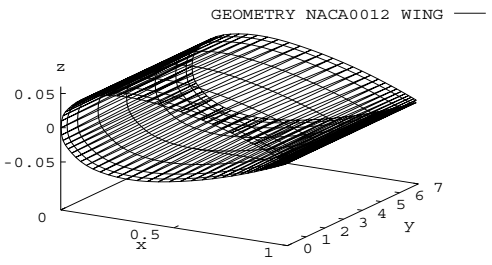

Figure 4: Geometry NACA0012 wing.

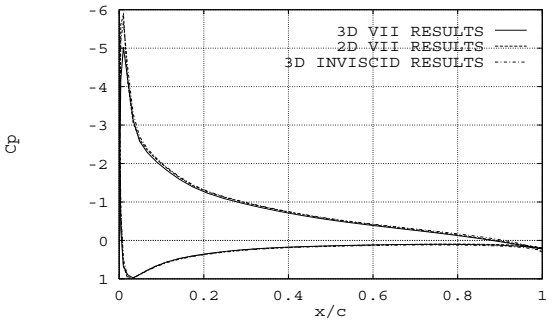

Figure 5: Comparison of inviscid and interactive 3D method, $\alpha = 11^o$, and 2D interactive method, $\alpha = 10^o$.

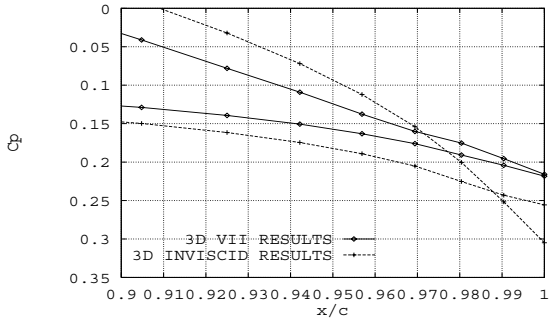

Figure 6: Comparison of 3D interactive results and 3D inviscid results near the trailing edge.

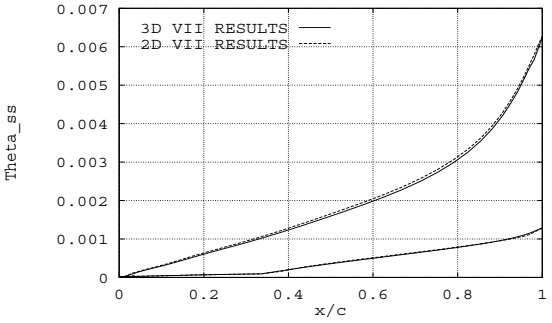

Figure 7: Comparison of 3D interactive method, $\alpha = 11^o$, and 2D interactive method, $\alpha = 10^o$.

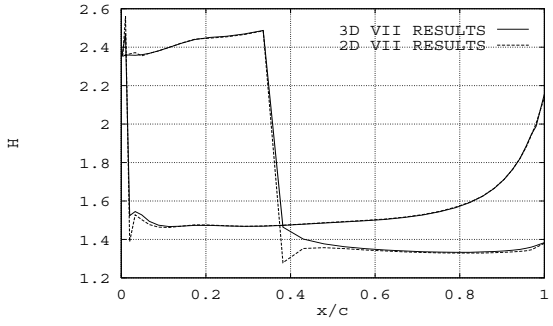

Figure 8: Comparison of 3D interactive method, $\alpha = 11^o$, and 2D interactive method, $\alpha = 10^o$.

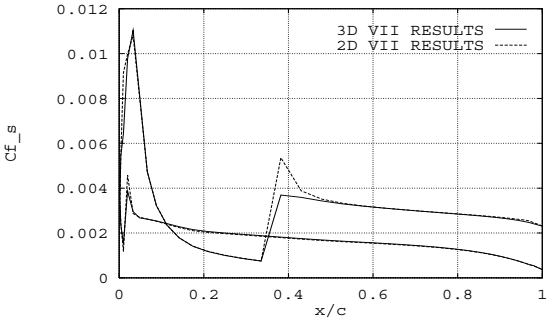

Figure 9: Comparison of 3D interactive method, $\alpha = 11^o$, and 2D interactive method, $\alpha = 10^o$

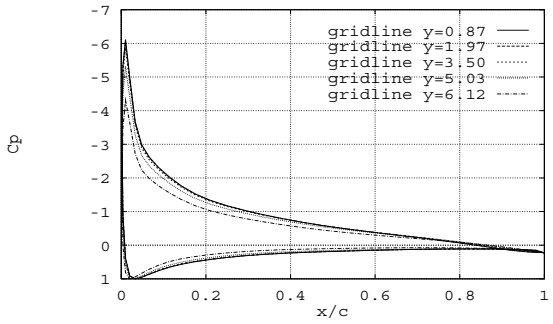

Figure 10: Comparison C_p at different spanwise stations, $\alpha = 12.5^o$.

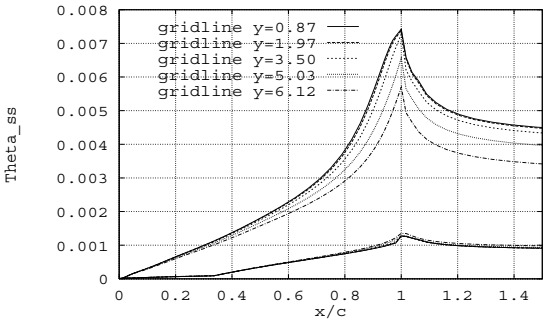

Figure 11: Comparison θ_{ss} at different spanwise stations, $\alpha = 12.5^o$.

that they are in good agreement. The computed shape factor and streamwise skin friction coefficient values are displayed in figures 8 and 9 and compare favourably with the two-dimensional data. Only in the transition region the results differ: in both cases transition has been tripped at the same location, however, a different finite differencing cell has been used at the transition point in the two programs.

6.2 Three-dimensional wing flow

By increasing the incidence beyond 11^o, three-dimensional effects become clearly present. Results in figures 10 to 15 are shown for an incidence of 12.5^o for which flow case there is a small region with separation present.

In figure 10 the pressure distribution is shown for five different chordwise stations, where gridline $y = 0.87$ lies close to the root, gridline $y = 3.5$ lies midwing and gridline $y = 6.12$ is close to the tip of the wing. Away from the root the pressure distribution decreases.

Figure 11 shows the streamwise momentum thickness for the various gridlines. The results near the root show a more severe growth of θ_{ss} near the trailing edge than the results closer to the tip. In figures 12 and 13 the shape factor and the streamwise skin friction coefficient are shown. From these graphs it is clear that the flow is separated in the trailing edge region close to the root. For gridlines $y = 0.87$ and $y = 1.97$ it is seen that $C_{f_s} < 0$ and $H > 2.73$.

Figure 14 shows the computed inviscid and interactive spanwise lift distribution, which differ significantly near the root. In figure 15 the global iteration process is plotted, in which quite a rapid error decay is seen.

The calculations have been performed on a HP unix work station and for the above flow case of separated three-dimensional wing flow 70 minutes of CPU time were required to converge.

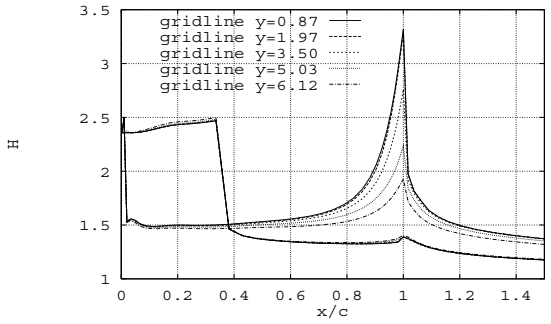

Figure 12: Comparison H at different spanwise stations, $\alpha = 12.5^o$.

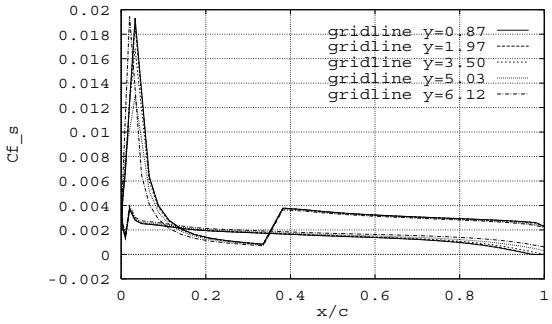

Figure 13: Comparison C_{f_s} at different spanwise stations, $\alpha = 12.5^o$.

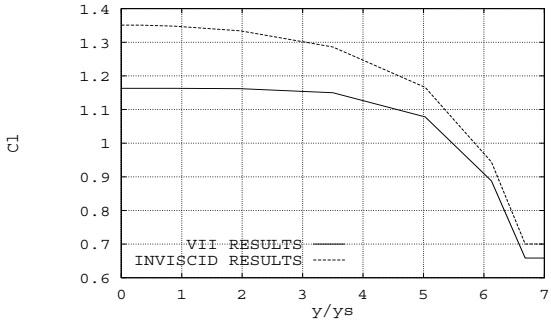

Figure 14: Comparison of inviscid and interactive 3D spanwise C_l distribution, $\alpha = 12.5^o$.

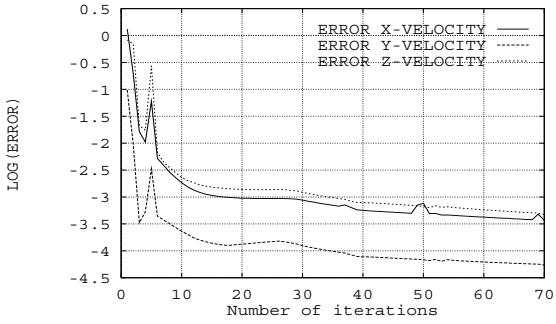

Figure 15: Error decay versus the number of iterations.

7 CONCLUDING REMARKS

Fully quasi-simultaneous coupling has been described for three-dimensional incompressible flow over wing configurations. Three interaction laws have been derived from the used Dirichlet panel method, and they have been integrated in the fully three-dimensional quasi-simultaneous scheme. Its capability of modelling (quasi-)three-dimensional flow, including separation, over an unswept NACA0012 wing is successful. The theory is to be further tested and improved to include swept wing calculations on non-orthogonal grids which will be useful for todays wing design.

Acknowledgements

The research was partly funded by the University of Bristol, UK, the Engineering and Physical Research Council, UK, and the Defence Evaluation and Research Agency, UK.

REFERENCES

[1] R.C. Lock and B.R. Williams, "Viscous-Inviscid Interactions in External Aerodynamics," *Progress in Aerospace Sciences*, **24**, 51-171 (1987).

[2] J. Cousteix and R. Houdeville, "Singularities in Three-Dimensional Turbulent Boundary-layer Calculations and Separation Phenomena," AIAA Paper 81-4201 (1981).

[3] P.D. Smith, "An Integral Method for Three-Dimensional Compressible Turbulent Boundary Layers," ARC R&M 3739 (1972).

[4] D.E. Edwards and J.E. Carter, "Analysis of Three-Dimensional Separated Flow with the Boundary-Layer Equations," AIAA paper 85-1499 (1985).

[5] M. Lazareff and J.C. Le Balleur, "Computation of Three-Dimensional Flows by Viscous-Inviscid Interaction Using the 'MZM' Method," AGARD CP-412, paper 25 (1986).

[6] J.C. Wai, J.C. Baillie and H. Yoshihara, "Computation of Turbulent Separated Flows over Wings," *Num. and Phys. Aspects of Aerodynamic Flows*, T. Cebeci (ed.), Springer-Verlag, 397-411 (1986).

[7] Fluid Dynamics Panel working Group 10, "Calculation of 3D Separated Turbulent Flows in Boundary Layer Limit," AGARD-AR-255, 1-3 (1990).

[8] A.E.P. Veldman, "New, Quasi-Simultaneous Method to Calculate Interacting Boundary Layers," *AIAA J.*, **19**, 79-85 (1981).

[9] D.E. Edwards, "Analysis of Three-Dimensional Flow Using Interacting Boundary-Layer Theory," *Proc. IUTAM Symposium on Boundary-Layer Separation*, F.T. Smith and S.N. Brown (eds.), Springer-Verlag, 163-178 (1987).

[10] A.J. van der Wees, J. van Muijden and J. van der Vooren, "A Fast and Robust Viscous-Inviscid Interaction Solver for Transonic Flow about Wing/Body Configurations on the Basis of Full Potential Theory," AIAA Paper 93-3026 (1993).

[11] B. Mughal and M. Drela, "A Calculation Method for the Three-Dimensional Boundary-Layer Equations in Integral Form," AIAA Paper 93-0786 (1993).

[12] K.D. Brown, "Computational Analysis of Flow Speed Axial Flow Rotors," PhD Thesis, Dept. of Aerospace Eng., University of Bristol (1997).

[13] P.R. Ashill, R.F. Wood and D.J. Weeks, "An Improved, Semi-Inverse Version of the Viscous Garabedian and Korn Method (VGK)," RAE TR 87002 (1987).

[14] J.E. Green, "Application of Head's Entrainment Method to the Prediction of Turbulent Boundary Layers and Wakes in Compressible Flow," RAE TR 72079 (1972).

[15] R. Houwink and A.E.P. Veldman, "Steady and Unsteady Flow Computations for Transonic Airfoils," AIAA Paper 84-1618 (1984).

[16] L. Morino and C.-C. Kuo, "Subsonic Potential Aerodynamics for Complex Configurations: A General Theory," *AIAA J.*, **12**, 2, 191-197 (1974).

[17] J.E. Kerwin, S.A. Kinnas, J.-T. Lee and W.-Z. Shih, "A Surface Panel Method for the Hydrodynamic Analysis of Ducted Propellers," *SNAME Transactions*, **95**, 93-122 (1987).

[18] A.E.P. Veldman, "Strong Viscous-Inviscid Interaction and the Effects of Streamline Curvature," *CWI Quarterly*, **10**, 353-359 (1997).

[19] E.G.M. Coenen, "Quasi-Simultaneous Coupling for Wing and Aerofoil Flow," *Domain Decomposition Methods in Sciences and Engineering*, C.-H. Lai, P.E. Bjørstad, M. Cross and O.B. Widlund (eds.), Domain Decomposition Press, Beyer, 197-205 (1999).